M. Rusconi, F. Ferrari, F. Topputo
*The Effect of a Rocky Terrain for Cubesat Landing on Asteroid Surfaces*
Advances in Space Research, Vol. 71, N. 1, 2023, p. 829-844
doi:10.1016/j.asr.2022.10.056

# The effect of a rocky terrain for CubeSat landing on asteroid surfaces

Martina Rusconi[a], Fabio Ferrari[b,a], Francesco Topputo[a]

[a]*Department of Aerospace Science and Technology, Politecnico di Milano, Via La Masa 34, 20256, Milano, Italy*
[b]*Space Research and Planetary Sciences, Physics Institute, University of Bern, Gesellschaftsstrasse 6, 3012 Bern, Switzerland*

**Abstract**

The paper describes a general modelling procedure to build a simulation tool to investigate contact motion of a CubeSat on an asteroid surface. We investigate landing performance and landing success for the case of elastic rocky terrain and flat surfaces. As a case study, we focus on the disposal of ESA's Hera Milani CubeSat by landing on the moon of Didymos binary asteroid system. The simulation environment includes the modelling of real shape and 6-DOF motion of the lander, the shape-based gravity models of Didymos and Dimorphos and rocks on surface, that are generated as physical obstacles. Trends and estimates on the performance of the landing phase and the most relevant effects on the outcome of the soil interaction process, are inferred. The statistical results on settling time, dispersion area and motion characteristics, such as number of bounces, show and quantify the effect of rocks on a successful passive and permanent landing.


*Keywords:* Ballistic landing; Asteroid; Contact dynamics; Simulation; Rocky terrain; AIDA

## 1. Introduction

Nowadays more than 27000 Near-Earth Asteroids (NEAs), whose orbit enters the Earth's neighbourhood, have been discovered and classified. The continuously updated population of near-Earth minor bodies is a large and accessible set of targets for space missions (Ferrari & Lavagna (2018), Ferrari et al. (2021a)). Asteroid research is attracting growing notice for scientific and economic reasons and for planetary defence (Rivkin et al. (2021)). From a scientific standpoint asteroids are considered leftovers of the formation process of the Solar System. Close-proximity missions can help refine the models and shed a light on the formation processes of these objects (Michel et al. (2016)). Asteroids are also considered a unique opportunity for In-Situ Resource Utilization (ISRU) technology development. To be effective, ISRU techniques require to fill the knowledge gap of mechanical, physical and environmental properties of small bodies. Direct interaction is the only way to determine detailed information (Michel et al. (2018)). Finally, attention is set on bodies threatening to impact the surface of the Earth. NEAs include Potentially Hazardous Asteroids (PHAs), classified based on the possibility of threatening impacts on the Earth. The design of effective mitigation strategies relies upon the knowledge of asteroid properties and their material interaction with man-made probes (Michel et al. (2016)).

Landing on a small body is a high-risk high-gain solution (Ferrari et al. (2021b)): the scientific information obtainable is balanced by critical issues and uncertainties in the design of the manoeuvre. The presence of small bodies with irregular mass distribution makes the dynamics of the satellite, that moves in the surroundings, highly chaotic (Ferrari & Lavagna (2018)). Moreover, there is little information on the physical characteristics of the surface during preliminary mission design (Ferrari & Lavagna (2018), Michel et al. (2016), Michel et al. (2018)). Considering these issues, we performed a statistical analysis on the effect of environmental parameters to investigate the performance of a landing disposal.

The paper describes the modelling of a CubeSat passive landing on the surface of the small moon of a binary system. The simulation campaign investigated the effect on landing performance of a rigid and elastic rocky terrain compared to a flat one, with

*Email addresses:* martina.rusconi@polimi.it (Martina Rusconi), fabio.ferrari@unibe.ch (Fabio Ferrari), francesco.topputo@polimi.it (Francesco Topputo)

no obstacles or soil irregularities. An irregular soil is typical of asteroids and a rigid and elastic terrain is a worst-case assumption. In fact, an undeformable soil performs low energy dissipation at impact, while a deformable regolith bed is associated to a low coefficient of restitution (Van Wal et al. (2019), Van Wal et al. (2017), Tardivel et al. (2014)), according to the contact model described in Section 3.5. In the specific case considered, a successful manoeuvre is targeted, with success identified as the capability for the lander to stay on the target surface. Goal is to estimate the influence of a rough soil on contact motion performance. The case studied is the end-of-mission transfer of Milani, a small CubeSat on board the upcoming Hera mission by ESA, by landing on Dimorphos, the moon of Didymos binary asteroid system. Hera is part of the Asteroid Impact and Deflection Assessment (AIDA) collaboration between NASA and ESA. We provide a general procedure to build a simulation tool for the analysis.

The article is structured as follows: first a brief overview of previous missions and literature on the topic in Section 1.1; then the case of study considered is presented in Section 2; the physical modelling of the problem is described through every component of the simulation building process in Section 3; the numerical implementation in the software and the simulation campaign carried out are given in Section 4; finally, the results obtained are presented, discussed and the main conclusions derived in Sections 5, 6 and 7, respectively.

### *1.1. Previous missions and studies*

No detailed information is available on the surface of Dimorphos (Naidu et al. (2020)), so we considered previous missions to similar bodies as baselines.

To date very few probes managed to land on a small body, was it to perform Touch And Go (TAG) operations or to rest permanently on the surface. NEAR-Shoemaker spacecraft ended its mission around the km-sized rocky asteroid 433 Eros with an unprogrammed landing (Antreasian et al. (2001)). Hayabusa spacecraft performed a completely controlled descent for TAG operations on S-type asteroid 25143 Itokawa of medium dimensions, approximately 330 m (Yano et al. (2006)). The follow-up mission Hayabusa2 deployed successfully two hopping rovers called MINERVA II 1A/B and the MASCOT lander on the half-km sized carbonaceous asteroid Ryugu (Tsuda et al. (2020)). The most recent mission targeting an asteroid is OSIRIS-REx, which performed TAG sampling on the medium-size C-type 101955 Bennu (Lauretta D.S. (2019)). Earlier, Rosetta's Philae lander performed the first soft-landing on the irregular nucleus of comet 67P/Churyumov-Gerasimenko (Jurado et al. (2016)). The landing trajectories analyzed in the literature of the previous missions have been mainly characterized in the aftermath, while the paper focuses on a preliminary analysis of the landing, when no accurate environmental data are available (Biele et al. (2015), Yano et al. (2006), Antreasian et al. (2001)).

Previous studies introduced modelling and simulation procedures to investigate the motion of probes approaching and moving on the surface of small bodies. Works as Tardivel et al. (2014), Van Wal et al. (2017) and Van Wal (2014) focused on the global landing performance of spherical probes, to ease calculations. However, Van Wal et al. (2019) and Zeng et al. (2022b) proved the non-negligible effect of a non-spherical shape on contact motion. The irregular mass distribution of small bodies is typically represented with the most accurate shape model available, such as a polyhedron one for Itokawa in Van Wal & Tardivel (2016) or Bennu in Van wal et al. (2018) and Wen et al. (2020). In Zhang et al. (2021) the combination of polyhedron models for both the small body and the lander, and consequently multi-contact dynamics of the lander analysed. Often, in a preliminary design there are no high-resolution shape models of secondary bodies of binary systems. Commonly, the shape models described assume constant density. The gravity field must be well represented in the proximity of the surface. Van Wal et al. (2017) and Van Wal et al. (2019) proposed solutions to lower the cost of gravity calculation related to a polyhedron model of the mass distribution, a resolution reduction has been also applied in Zhang et al. (2021). Surface features can be included to perturb the motion, they are modeled in Tardivel et al. (2014) with a stochastic approach, while in Van Wal et al. (2017) and Van Wal & Tardivel (2016) as physical obstacles through the persistent rocks generation technique. Due to the high uncertainty on the physical characteristics of the environment, the typical approach exploits an impulsive model for contact event solution on a hard terrain: the collision is of infinitesimal duration and modelled through impulses acting at contact point (Van Wal et al. (2019), Tardivel et al. (2014)). Differently, when focus is set on the interaction with a regolith soil, Van wal et al. (2018) suggests carrying out specific Discrete Element Method (DEM) analyses.

The study of the text fits in the literature on the topic described, that is currently growing interest. Another recent similar study that applies different methods can be found in Zeng et al. (2022a). The paper provides an approach that combines the real shape of the CubeSat, the most accurate shape and gravity models available for the case at hand and rocks generated as physical obstacles. The techniques adopted are taken from literature examples: arbitrary shapes of the satellite have already been studied in Van Wal et al. (2019) and Zeng et al. (2022b) and the rocks generation method comes from Van Wal et al. (2017). These elements are put together to adequately analyse the landing phase to an original target: the smallest secondary body ever targeted to date, by considering the full 6-DOF dynamics of the case studied. We focused on the final descent and impulsive interaction with the terrain. In particular, we investigated the effect of rocks on landing performance. The results obtained will be valuable to understand the contact dynamics of a small satellite on a small body in a binary system and will provide performance estimates for Milani's landing.

## 2. Case of study

The analysis is carried out in the context of the AIDA collaboration between NASA and ESA. ESA's Hera mission will carry and deploy CubeSats Milani and Juventas in the proximities of the target, Didymos binary asteroid system (Cheng et al. (2015)). Hera is a self-standing mission to be launched

Table 1. Physical and dynamical properties of Didymos system of asteroids. Note: The orbital elements are given at epoch 2457000.5 (2014-Dec-09.0).

| **Parameter** | **Value** |
|---|---|
| Heliocentric eccentricity | $0.383752501 \pm 7.7 \times 10^{-9}$ |
| Heliocentric semi-major axis | $1.6444327821 \pm 9.8 \times 10^{-9}$ AU |
| Heliocentric inclination to the ecliptic | $3.4076499 \pm 2.4 \times 10^{-6}$ ° |
| Rotation period of the primary | 2.2600±0.0001 h |
| Secondary orbital period | 11.920+0.004/-0.006 h |
| Distance between the centre of primary and secondary | 1.18+0.04/-0.02 km |
| Diameter of primary | 0.780 km ±10% |
| Diameter of secondary | 0.163±0.018 km |
| Dimorphos semi-major axes of ellipsoid representation $(\alpha, \beta, \gamma)$ | (103, 79, 66) m |
| Total mass | $5.278 \times 10^{11} \pm 0.54 \times 10^{11}$ kg |
| Mass parameter | $9.214 \times 10^{-3}$ |
| Didymos primary mass | $5.2294 \times 10^{11}$ kg |
| Dimorphos mass | $4.8631 \times 10^{9}$ kg |
| Bulk density of the primary | 2104 $kgm^{-3}$ ± 30% |
| $J_2$ parameter of primary body | 0.012 |

in 2024 following the NASA's Double Asteroid Redirection Test (DART), launched in November 2021, that performed a kinetic impact on the secondary body of the system, Dimorphos (Cheng et al. (2018)). Hera will characterize the impact effects and deploy the deep space CubeSats to complement its measurements (Michel et al. (2018)). Milani is a 6U-XL CubeSat of wet mass 12 kg and dimensions 365.9×226.3×100mm, with two sets of solar panels. A ballistic soft-landing on Dimorphos, targeting the DART crater site or its proximity, is being considered for disposal. Landing on target's surface would highly increase the scientific return of the mission. However, the manoeuvre is still an option to be investigated due to the critical issues it presents (Ferrari et al. (2021a)). In the analysis performed the goal of the landing was to stay on surface after contact, but the actual purpose of such a disposal is still undefined. The paper focuses on one specific option. Dimorphos is the smallest asteroid to be targeted by a space mission to date and the first one that is part of a binary system (Cheng et al. (2018), Michel et al. (2018)), both factors make the landing manoeuvre challenging. Its gravity field is very weak on surface: around $10^{-4}$ - $10^{-5}$ $m/s^2$ and escape velocity is estimated with average order of magnitude of few cm/s (Ferrari et al. (2021a), Ferrari & Lavagna (2018), Laino (2021)). Moreover, the dynamical environment generated in the surroundings by the asteroids is highly chaotic due to the combination of effects of the two attractors (Ferrari & Lavagna (2018)). Dimorphos orbits the primary on a quasi-circular path at a distance of 1180m in approximately 11.9h. The moon's rotation is assumed in a synchronous 1:1 spin-orbit resonance, similarly to other observed binaries (Michel et al. (2016)). The target is spectroscopically classified as Sq-type, chondrite-like (Cheng et al. (2015)). The physical characteristics of the body are mainly obtained from ground-based observations. Table 1 reports Dydimos system properties.

## 3. Physical problem modelling

To accurately reproduce the final descent of the satellite passive landing and its interaction with surface, it is crucial to model the micro gravity near surface and the characteristics of the terrain, both in terms of soil profile and of mechanical properties (Ferrari & Lavagna (2018), Van Wal et al. (2017), Tardivel et al. (2014)).
The simulation set-up originates from the available literature on contact dynamics and surface motion on small bodies, and extends their validity within the limitations of the present work. The full 6-DOF translational-rotational dynamics is considered. Each element is modelled applying adequate techniques selected from trade-off analyses between the methods in the literature. Main drivers for the choices have been accuracy and realism and a compromise with the computational capabilities available.
The implemented method adopts the real shape of the CubeSat that moves in the dynamical environment generated by the binary system and interacts with a hard and rigid soil, which is assumed flat in an extreme case scenario of highly elastic terrain or with rocky elements generated as physical obstacles to the surface motion. The paper focuses on these possible terrain configuration and investigates their influence on the contact motion.

### *3.1. Dynamics*

The final landing phase includes ballistic flight, collision event and continuous surface motion. The lander's state variables are propagated with respect to a body-fixed frame, in Figure 1, centred in Dimorphos' barycentre and aligned to its principal axes of inertia, based on the examples in Van Wal et al. (2019), Van Wal et al. (2017), Van Wal & Tardivel (2016) and Tardivel et al. (2014) about Itokawa. A typical assumption is

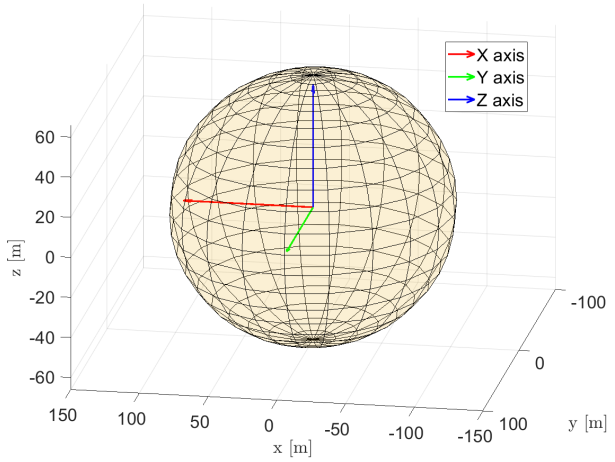


Fig. 1. Fixed body reference frame on Dimorphos, centred in Dimorphos' barycentre and aligned to its principal axes of inertia. x-axis is aligned and opposite to Didymos primary, the z-axis is assumed aligned to the spin axis of the asteroid and the y-axis is assumed aligned to Dimorphos velocity.

uniform rotation of the asteroid (Van Wal et al. (2019), Van Wal et al. (2017), Van Wal & Tardivel (2016) Tardivel et al. (2014)).

Gravitational attraction is the dominant force acting on the CubeSat when close to the asteroid surface (Ferrari & Lavagna (2018), Van Wal et al. (2017)). Contact dynamics simulation propagates in time scales low enough that external perturbing forces, such as solar radiation pressure, can be considered negligible for such small times of flight (Van Wal et al. (2019), Van Wal et al. (2017), Tardivel et al. (2014), Van Wal & Tardivel (2016)). From previous considerations the fundamental dynamics equation 1 describes the lander's centre of mass linear acceleration in the body-fixed rotating frame (Wen & Zeng (2022), Scheeres et al. (2019)).

$$\begin{aligned}\vec{a}_{CG} =& \vec{g}_{D2}(\vec{r}) + \vec{g}_{D1}(\vec{r}_{D1} - \vec{r}) + \vec{g}_{tidal}(-\vec{r}_{D1}) + \\ &- \vec{\Omega} \times (\vec{\Omega} \times \vec{r}) - 2\vec{\Omega} \times \vec{v} + \frac{1}{m}\vec{F}_c\end{aligned} \tag{1}$$

External actions on the satellite are gravitational attraction of the two asteroids $\vec{g}_{D1}(\vec{r}_{D1} - \vec{r}) + \vec{g}_{D2}(\vec{r})$, dependent on the probe state $\vec{r}$ and on the primary position with respect to the frame fixed in Dimorphos $\vec{r}_{D1}$, the tidal acceleration term $\vec{g}_{tidal}(-\vec{r}_{D1})$ and centrifugal and Coriolis terms due to Dimorphos' rotation, and contact forces ($\vec{F}_c$), which equal zero during ballistic flight.

### 3.2. Probe and asteroid bodies

Probe shape's simplification is acceptable when dealing with global landing trajectory design (Ferrari & Lavagna (2018), Laino (2021)). However, studies from Van Wal et al. (2019), Van Wal et al. (2017) and Zeng et al. (2022b) proved that lander shape effect when focusing on surface motion performance is non negligible. The higher computational cost is justified by better representativeness of the results. Hera mission design is at an advanced stage, so Milani's definitive configuration is available and simulated in Figure 2: a 6U CubeSat with two sets of deployed solar panels, which cannot be retracted. Two

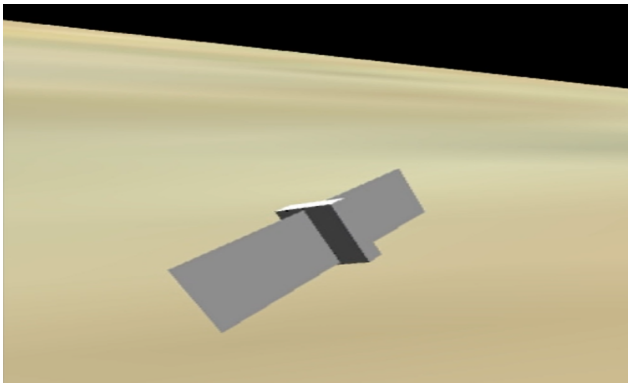

Fig. 2. Milani CubeSat shape in the simulation environment.

important approximations are: uniform mass distribution and rigid solar panels, whose realistic representation and effect are beyond the scope of this work.

Since the realistic shape of the CubeSat is considered, the 6-DOF dynamics is solved in the simulation. The attitude models and equations of the software described in Section 4 have been exploited. A complete explanation is available in the documentation of Project Chrono. The body is modelled as rigid and the baseline attitude equations of motion are reported as reference. Equation 2 defines the angular velocity ($\vec{\omega}$) evolution of the satellite in its local frame, with given inertias (**I**), and equation 3 the kinematics evolution of quaternions ($\vec{q}$). The torque effect of the asteroids' gravity field is not considered in the analysis, because assumed negligible with respect to the contact actions. The term $\vec{T}_{contact}$ defines the rotational effect on the lander caused by the interaction with the surface. The software automatically deals with reference frames conversions to integrate the attitude motion. The initial body angular velocity in local frame, initial attitude quaternions and mass properties are taken as inputs by the software to set up the rigid body of the lander, the reference frame in which each parameter is defined is declared by the user and the software automatically imposes frames conversion to keep consistency in the integration of the equations of motion. Since the embedded models of the software are exploited to solve for the contact dynamics, the reader is referred to the available documentation of the software for a more detailed explanation. The equations of motion are given as qualitative representation of the analysis performed, in which the complete 6-DOF dynamics is solved for with the software.

$$\dot{\vec{\omega}} = -\mathbf{I}^{-1}(\vec{\omega} \times \mathbf{I}\vec{\omega}) + \vec{T}_{contact} \tag{2}$$

$$\dot{\vec{q}} = \frac{1}{2}\mathbf{B}(\vec{q})\begin{bmatrix}0\\ \vec{\omega}\end{bmatrix} \tag{3}$$

Target's high-resolution shape representations allow to model the surface configuration of the terrain (Van Wal et al. (2017)), which influences the collision detection as the relative distance of the surface with any point of the satellite goes to zero, and the local normal inclination, which influences the contact dynamics model, at the expense of a larger computational

cost than simpler shapes. Data availability limits modelling options for target shape. In fact, models inferred from ground-based observations are highly uncertain (Michel et al. (2018), Michel et al. (2016)). Considering Didymos binary system, the primary is sufficiently large that a polyhedron shape model has been derived for it, while Dimorphos' can only be approximated as a tri-axial ellipsoid (Ferrari & Lavagna (2018)) from semi-major axes estimates in Table 1 and shown in Figures 1 and 3. As proved by the literature, a polyhedron model for Dimorphos would have been beneficial to the study, however the flat ellipsoid model was the only available. The flatness of the surface influences the evolution of the lander dynamics when impacting the ellipsoid because the local normal defines the direction in which the contact impulses act and the absence of irregularities on surface influences the collision detection when the lander approaches Dimorphos. The drawback of low realism of surface configuration can be reduced including an independent model for terrain rendering. On the other hand, a flat ellipsoid model is computationally beneficial in terms of cost and collision detection evaluation and solution. There is no reason to implement cost-reduction techniques to ease the shape interactions computations, such as the Signed Distance Field (SDF) in Van Wal et al. (2019). Since the target is Dimorphos and the analysis focuses on the interaction with its surface, Didymos primary is only modelled as an external action on the satellite, even if a higher resolution model is available.

### 3.3. Gravity

The irregular shape and mass distribution of an asteroid cause a chaotic dynamical environment in its surroundings and the gravity field varies locally on the surface. Moreover, gravity approximations may diverge in the close-proximity of the attracting body (Van Wal et al. (2017)). The lander descent near surface happens inside the Brillouin sphere, this makes the shape-based gravity field representation the most favourable solution (Laino (2021)). Data availability has been the main driver to choose the tri-axial ellipsoid shape-based approach. Dimorphos' attraction evaluation is based on the work by Scheeres (1994). Given the gravity potential definition through elliptic integrals in Eq. 4

$$
\begin{aligned}
U_{D2} &= -\frac{3}{4}\mu_{D2}\int_{\lambda(\vec{r})}^{\infty}\frac{\phi(\vec{r},u)}{\Delta(u)}\,du \\
\phi(\vec{r},u) &= \frac{r_x^2}{u+\alpha^2}+\frac{r_y^2}{u+\beta^2}+\frac{r_z^2}{u+\gamma^2}-1 \\
\Delta(u) &= \sqrt{(u+\alpha^2)(u+\beta^2)(u+\gamma^2)} \\
\lambda(\vec{r}):&\quad \phi(\vec{r},\lambda)=0
\end{aligned}
\tag{4}
$$

gravity acceleration is derived as its gradient as in Eq. 5.

$$
\begin{aligned}
\vec{g}_{D2} &= \nabla U_{D2}(\vec{r}) = \\
&= \begin{cases}
-\frac{3}{2}\mu_{D2} r_x \int_{\lambda(\vec{r})}^{\infty}\frac{1}{(u+\alpha^2)\Delta(u)}\,du \\
-\frac{3}{2}\mu_{D2} r_y \int_{\lambda(\vec{r})}^{\infty}\frac{1}{(u+\beta^2)\Delta(u)}\,du \\
-\frac{3}{2}\mu_{D2} r_z \int_{\lambda(\vec{r})}^{\infty}\frac{1}{(u+\gamma^2)\Delta(u)}\,du
\end{cases}
\end{aligned}
\tag{5}
$$

The force is punctually evaluated at each time step applying the model described at the current position.
The target is part of a binary system, so the gravity of the primary must be included , along with the tidal effect caused by the primary attraction on the secondary (Wen & Zeng (2022)). Didymos primary is represented only through its effect on the dynamics due to the large distance between the two asteroids with respect to the length scale of the simulation. The work in Ferrari & Lavagna (2018) proved that, at the position of Dimorphos, approximating Didymos' gravity field by that of a point source is similar to the polyhedron shape result. Consequently, a central field superimposed with spherical harmonics up to order 2, given the data in Table 1 (Zannoni et al. (2018)), has been used as an acceptable compromise between computational cost and accuracy. Eq. 6 reports the definition of the gravity potential when the spherical harmonics' model up to order 2 is considered. To take into account the attraction of the primary to both the lander and the secondary, the gravity acceleration terms in Eq. 7 are computed at the lander position with respect to Didymos and at the primary position with respect to the secondary, with opposite signs, accordingly to the sign convention introduced in Eq. 6.

$$
U_{J2} = -\frac{\mu_{D1}}{r}\left[1 - J_2\left(\frac{R_P}{r}\right)^2\frac{1}{2}\left(3\left(\frac{r_z}{r}\right)^2-1\right)\right] \tag{6}
$$

$$
\vec{g}_{D1} + \vec{g}_{tidal} = \nabla U_{D1}(\vec{r}_{D1}-\vec{r}) + \nabla U_{D1}(-\vec{r}_{D1}) \tag{7}
$$

Simulating the forces on Milani in a trajectory nominally targeting the DART crater, the secondary body is proved the major influence on the dynamics, with average magnitude of gravity force roughly $1\times10^{-3}$ - $1\times10^{-4}$N, closer to $1\times10^{-3}$N. However, Didymos primary has non-negligible effect of order of magnitude $1\times10^{-4}$N. The apparent rotation force due to asteroid spin has a minor effect than the other influences, it includes both centrifugal and Coriolis contribution and has order of magnitude of $1\times10^{-5}$ - $1\times10^{-6}$N.

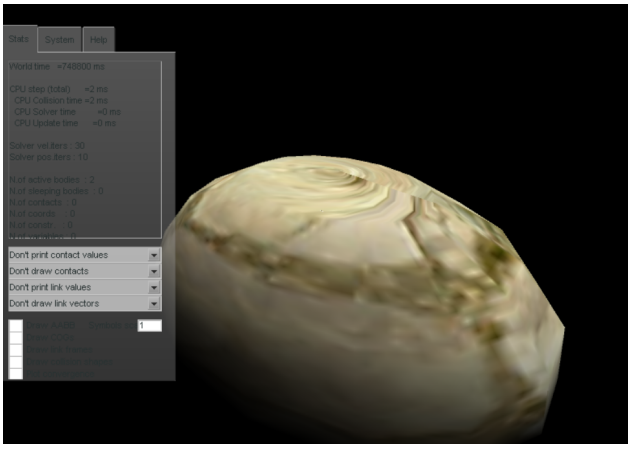


Fig. 3. Dimorphos ellipsoidal shape in the simulation environment. (Note: the Figure is taken from Project Chrono simulation rendering tool, the grey box on the left side can be ignored for the purposes of the Figure).

### 3.4. Surface features

We introduced a specific model to simulate surface features of Dimorphos to compensate for the flatness of the ellipsoidal shape. The lander is not designed specifically for landing on Dimorphos surface (Ferrari et al. (2021a)), whose morphology is highly uncertain. This variability has an important effect on the probe's dynamics (Tardivel et al. (2014), Van Wal et al. (2017)). A rigid rocky terrain has been simulated in view of an extreme case scenario approach compared to a soft regolith layer. The rocks generation technique in Van Wal et al. (2017) and Van Wal & Tardivel (2016) procedurally creates rigid bodies and puts them on the surface of the target crossed by the lander to simulate rocks and obstacle the trajectory of the probe. It is preferable to the stochastic model in Tardivel et al. (2014) and Van Wal (2014), that simulates the effect of rocks as random impulses applied to the probe dynamics on surface, because the elements created are physical obstacles to lander's motion, which can bounce on a rock or lean on it. This improves the realism and balances the lack of data on rocks distribution on Dimorphos, for which we make assumptions from similar asteroids. In our simulation tool, rocks are modelled as rigid bodies as well. Due to the huge memory and computational cost required to simulate many single rocks over all the asteroid ellipsoid, the rocky area has been limited to a local surface world near the satellite. The region is defined as a grid on the ellipsoid, centred in the crater site, with each cell of 10° side in latitude and longitude. Rocks are icosahedra with maximum 12 vertices. Mean dimensions are computed randomly from a Zhang distribution based on minimum and average chord inputs (Zhang et al. (1999)), which are taken from literature data about Itokawa in Van Wal et al. (2017) and Tardivel et al. (2014) and the classification of Dimorphos gravel elements in Michel et al. (2016). Data are given in Table 2. Since granular media effects are not investigated, the possible size of rocks is lower bounded, while no real limit is put on large blocks, in fact the ellipsoid shape model does not represent eventual big masses on the surface, which can affect lander's motion. Rocky elements are randomly generated, positioned and oriented on the surface of each active cell. The seed of random number generation is controlled to get always the same terrain pattern in the same area in different simulations. The density of rocks distribution comes from visual inspection, similarly to the work in Van Wal et al. (2017), and a compromise between realism and computational time. One important assumption is that the elements do not work as gravitationally attracting masses, which is however reasonable for the Dimorphos case study, and considering the small times of flight between bounces.

### 3.5. Contact Dynamics

Crucial to satellite's dynamics is surface collision detection and solution. These require specific models and a local frame centred in the contact point and axes aligned with the local normal and terrain's tangential directions, as in Figure 4. First, contact between the two bodies is detected when the relative distance between them goes to zero. Probe shape selection and surface configuration modelling influence the distance calculation. Satellite structure and terrain physical properties influence

Table 2. Input parameters to generate rocky elements on Dimorphos surface.

| Parameter | Value |
|---|---|
| Minimum chord | 0.05m |
| Average chord | 2m |
| Number of rocks generated per surface cell | 100 |
| Number of active cells | 16 |

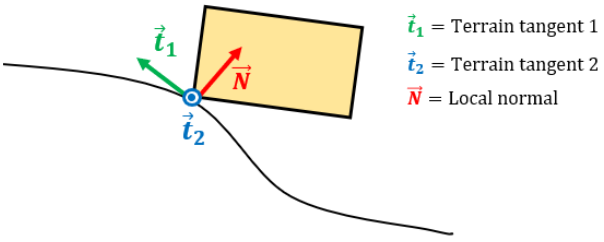


Fig. 4. Contact point reference frame example.

the collision forces modelling. Given the goals of the study, an extreme case scenario is assumed: interaction of the satellite with a hard terrain, which results in low energy dissipation at touch down. Differently, high dissipation would help avoiding escape from the target gravitational attraction after bouncing and decrease of the dispersion area on surface, which can be critical on small asteroids as Dimorphos. Contact forces acting on the lander during collision and continuous surface motion involve several effects whose complicate interaction is hardly reproducible (Van Wal et al. (2019), Van Wal et al. (2017)). Stronge model represents impact as a general eccentric impulsive collision and it is mostly used in previous works (Van wal et al. (2018), Van Wal et al. (2019), Van Wal & Tardivel (2016)). The main assumptions of Stronge model are:

- contact in an infinitesimal region;
- rigid and non-deformable impacting surfaces;
- immobile asteroid surface;
- impulses act at contact point to vary the satellite velocity and rotation states;
- impulses parametrized by scalar coefficients.

Impulse forces acting at collision instant have a normal component and a tangential one, with respect to the local soil inclination. The normal impulse enforces the non-penetrability condition, which can be parametrized through a scalar coefficient. The Coefficient Of Restitution (COR) measures the energy dissipation due to the normal impulse effect of the terrain and structure deformation: the lower the COR the more energy is dissipated. There is not a unique definition for the coefficient of restitution, Stronge defines it energetically in Van Wal et al.

(2019), while the Newtonian kinetic definition is applied in Tardivel et al. (2014), for example. The software exploited for the analysis defines it automatically and it is hardly obtainable outside the embedded algorithm, while the definitions applied in the post-process of the data are given in Section 5. The tangential component of the impulse is caused by friction, which is described by Coulomb model and the associated Coefficient Of Friction (COF). Implementing the realistic shape of Milani causes coupling between the two effects (Van Wal et al. (2019)). The reference equations used to model the contact dynamics are given in Section 4, to clarify the contact model embedded in the software that is exploited for the analysis. Scalar coefficients depend on shape, mass, surface physical properties and state of the impacting bodies (Van Wal et al. (2019), Van wal et al. (2018)). They can be estimated from the available data, from previous similar missions or from experiments, scaling the results to asteroid's environment. High uncertainty is associated to Dimorphos COR, while Milani's structure has already been designed, so its COR is estimated at 0.6 (Ferrari & Lavagna (2018)). Previous studies showed the dominant effect of the COR and the minor effect of the COF on the contact dynamics (Van wal et al. (2018), Van Wal (2014), Tardivel et al. (2014), Van Wal et al. (2017)). After the bouncing dynamics, the satellite can be at rest or begin surface continuous contact motion. Stronge's model originates from impulsive collision considerations, happening in an infinitesimal amount of time. Same actions can be applied during continuous contact motion on the surface, generalizing the model following the example from Van Wal et al. (2019).
Since contact action is just split into non-penetrability normal reaction force and friction, parametrized through scalar coefficients, these are the only parameters required to model the collision event.

## 4. Numerical implementation

We used Project Chrono (Tasora et al. (2016)) as a simulation tool. Chrono is a library with a modular interface, typically used for multi-body and granular dynamics problems. The software derives the underlying equations of motion from the environment set-up by the user. The default solver calls a symplectic semi-implicit Euler integrator to propagate the dynamics at each time step, which is set equal to 0.1 seconds. Translational dynamics of the lander is based on equation 1, while the rotational dynamics of equation 2 is automatically set up and solved within the Chrono's contact model exploited and later defined.
Collision shape, an envelope surrounding the physical item, must be defined to activate collision detection on a body in Project Chrono. In particular the outward margin, provided by this additional external shape added to the colliding bodies, allows the software to anticipate impacts. In fact, numerical schemes must anticipate the instants of contact, it would be inaccurate to solve for the dynamics of interpenetrated bodies, as explained in the software online tutorials. A triangular mesh surrounding Milani is considered to match the lander's collision shape and the actual shape. A collision envelope is given also to the asteroid and each rock on it. Contact happens when the distance between two bodies falls under a default threshold. The collision shape of Chrono exploits two default collision tolerances. An outward safe envelope around the body to define the volume of potential contacts' research; if at the beginning of a time step the envelopes of two bodies are not in contact and at the end of it they are interpenetrated, a collision is given to that time step. An inward margin limits the acceptable interpenetration in a step; in case of excessive interpenetration, the solver moves back to a slower algorithm for collision detection. Chrono contact detection algorithm has two subsequent phases. Broad phase is applied at each time step, and is used to broadly separate couples of possibly colliding bodies and not. Axis Aligned Bounding Boxes (AABBs) divide the tridimensional space occupied by a body, while the simulation environment is divided in bins; when two bounding volumes touch the same space bin in a time instant a possible collision is detected. The successive phase is called narrow phase and is solved only when there is a possible collision and the default algorithm accurately calculates the relative distance between two convex shapes, applying the Minkowski Portal Refinement method. When two shapes are found to interpenetrate within a default tolerance in a time step, a collision point is detected (Ferrari et al. (2019)). We use the Non-Smooth Contacts (NSC) method embedded in Chrono to solve for point contact dynamics. The effect of the contact forces is solved for the full 6-DOF dynamics of the lander, so both translational and rotational states after contact are automatically computed by the algorithm. In this model, collisions are impulsive and between hard and rigid bodies, so same assumption of Stronge model baseline. In particular, NSC implements a complementarity approach, by solving a DVI (Differential Variational Inequality) problem at each time step when contact is detected (Tasora & Anitescu (2010)). Similarly to the model in Section 3.5, the contact forces applied in a single time instant are a normal one to enforce non penetrability and a tangential one for Coulomb friction effect, with slip and stick automatically dealed with by the algorithm. In our analysis, we used the same value for COF in slip or stick. The normal force at contact ($\vec{F}_N$, and its magnitude $F_N$) is defined as in equation 8a, directed as the local normal unit vector $\vec{N}$. The complementarity condition in equation 8b is enforced: when the distance between colliding bodies ($\phi$) is positive the normal force is zero, while if a collision happens and the distance is considered zero, the normal force is non zero.

$$\vec{F}_N = F_N \vec{N} \tag{8a}$$

$$F_N \geq 0, \quad \phi \geq 0, \quad F_N \phi = 0 \tag{8b}$$

The tangential effect $\vec{F}_t$ (equation 9a) is modelled as Coulomb friction in equation 9b, with the COF symbol $f$. The force is collinear and opposite to contact point tangential velocity $\vec{v}_t$ (see equation 9b) and both stick and slip conditions are considered in equation 9d.

$$\vec{F}_t = F_{t_1} \vec{t}_1 + F_{t_2} \vec{t}_2 \tag{9a}$$

$$f F_N \geq \sqrt{F_{t_1}^2 + F_{t_2}^2} \tag{9b}$$

$$\vec{F}_t^T \vec{v}_t = -\|\vec{F}_t\|\|\vec{v}_t\| \tag{9c}$$

$$\|\vec{v}_t\|(fF_n - \sqrt{F_{t_1}^2 + F_{t_2}^2}) = 0 \tag{9d}$$

Non-linear constraints are relaxed, friction is modelled through the maximum dissipation method, to obtain an equivalent Cone Complementarity Problem. At each time step the problem is solved iteratively to get reaction forces and the new lander's state. A more detailed explanation of the embedded algorithms is in the software online tutorials and articles (Mazhar et al. (2013)).

The same material properties are assumed for asteroid and rocks and others for the lander. A note is due on the COR definition, the values for lander and terrain given to Chrono are used to solve impulsively one single contact and are not the same parameters derived in the post-process discussed in Section 5, that consider the global impact event from multi-contact 6-DOF dynamics of the lander.

In each simulation, from initial conditions on position, velocity and orientation, the lander moves in the dynamical environment of the binary system gravity field to the target asteroid. The motion is reconstructed in the proximity of the surface propagating the ballistic equations of motion; when the default collision condition is satisfied contact is detected and the probe configuration after impact is obtained solving the impulsive contact dynamics. After each collision the lander can bounce back on a ballistic arc or continue surface motion until it successfully comes to rest on the asteroid.

### *4.1. Computational capability*

Three sets of simulations (S1, S2, S3), whose input parameters are defined in Table 3, have been performed. 300 samples have been simulated for the S1 set that considers a flat surface, 100 samples for the S2 set, due to the higher computational cost required by rocks generation, and the S3 set includes 500 samples, divided in 5 sub-sets of 100 simulations each targeting different surface sites. Computational capabilities and time constituted a limit to the analysis performed. The number of samples analysed in each set was selected as a compromise between the necessity to have a sufficiently large population to infer statistical trends and the necessity to have a limited computational time. The generation of rocks in the S2 and S3 sets highly increased the simulation time. This drove the decision to limit the rocky area simulated in Chrono, as said in Section 3.4. In fact, it took less than 1 minute to complete one simulation in the S1 set, while approximately 15 minutes per sample were needed when rocks were generated in the S2 and S3 sets. In future updates the computational efficiency of the analysis can be optimized by improving the computational capability available and through more efficient coding, such as inserting a break of the simulation when the threshold for successful landing is crossed.

### *4.2. Simulation Campaign*

The initial conditions of the simulation campaign are based on the data available for the case at hand and previous similar studies. In particular, Milani Cubesat is required to target the DART crater site on the surface, or its surroundings, to infer the impact effects with onsite measurements. Nominal crater coordinates to date are (0°, 90°), given in the format (latitude, longitude), with 0° longitude at meridian crossing x-axis of minor inertia of Dimorphos in Figure 1.

To focus on the effect of a rocky soil on landing performance, we performed a simulation campaign with two sets of simulations, where the probe moves on a flat and a rocky terrain, respectively, with equal initial conditions of highly elastic soil. In the S1 set Dimorphos surface is a flat and rigid ellipsoid, as in Figure 3. The terrain COR is close to Itokawa's one found in literature as an extreme case and equal to 0.85 (Yano et al. (2006)). The region of possible initial positions of Milani, in longitude and latitude coordinates, is chosen to target the DART crater site or its proximity. The mean crater diameter's typical estimates are around 17m (Michel et al. (2016)). From proportionality considerations, approximating the elliptic perimeter of the surface as a circumference, a grid cell of 10° on Dimorphos is estimated to be 16m long. So, a square area of 40° side surrounding the nominal crater coordinates is considered and shown in Figure 5.

In the S2 set surface rocks are included and generated as detailed in Section 3.4. Rocks slow down the code execution, so these are added to a limited area in the surroundings of the targeted DART crater in Figure 6, and equal to the region of possible initial positions of S1 set.

The terrain COR is still 0.85 to infer direct comparison between S1 and S2 results. The latitude and longitude intervals, for the selection of initial lander coordinates in a simulation, are reduced of 5° on each side in Figure 7, to keep the initial contact with the surface inside the rocky area. The choice was based on the results about average distance travelled in S1 set, where most of the samples cover less than 5° on surface. Comparing the results of S1 and S2 simulations, the effect of a rocky terrain with respect to a flat one is inferred. Even if the rocky area simulated is limited, the samples in S2 mainly move inside

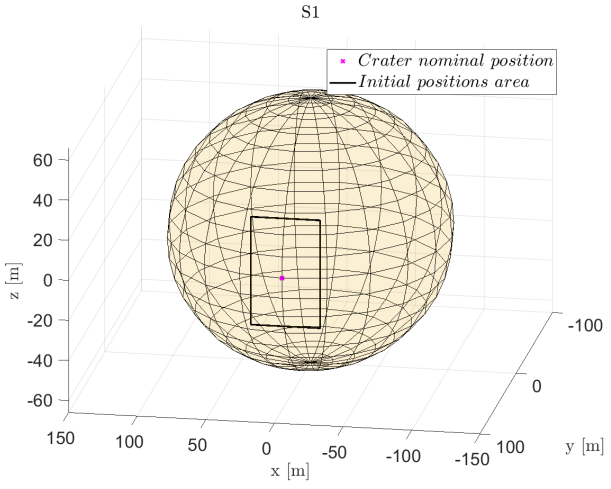


Fig. 5. Area of possible initial latitude and longitude coordinates in S1 set on the ellipsoid. The area is centered in the DART crater position at (0°, 90°), along the y-axis of the body-fixed frame.

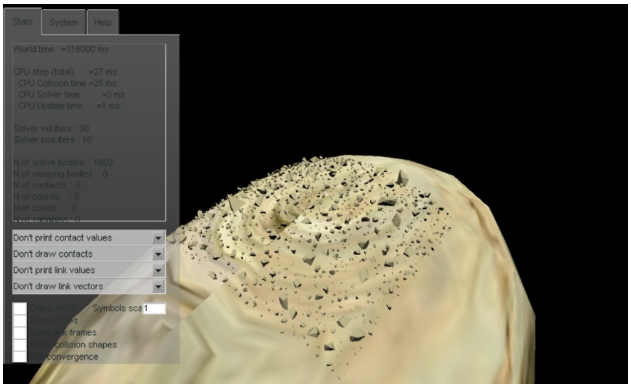

Fig. 6. Rocky terrain area simulated on Dimorphos ellipsoid in Project Chrono environment. (Note: the Figure is taken from Project Chrono simulation rendering tool, the grey box on the left side can be ignored for the purposes of the Figure).

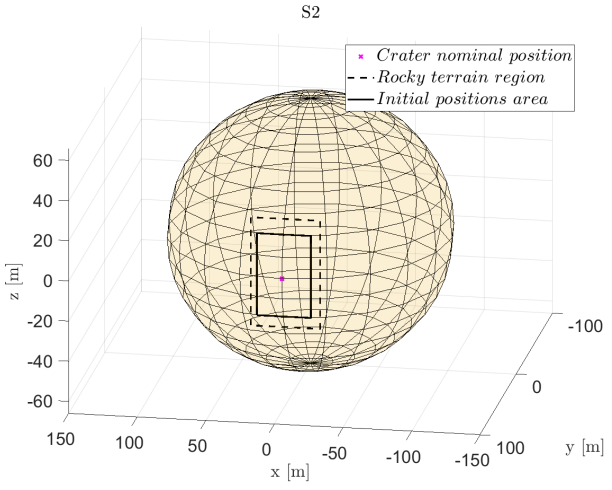


Fig. 7. Area of possible initial latitude and longitude coordinates in S2 set, delimited by the solid line. Rocky area inside the dotted line. Both centered in the DART crater site at (0°, 90°), along the y-axis of the body-fixed frame.

the region.

A third set of simulations, S3, investigates the effect of local terrain configuration. Rocks are generated on the same region of S2 and the initial probe position is kept fixed, targeting 5 different sites on surface in consecutive sub-sets of samples. The initial coordinates are shown in Figure 8. The targeted points right underneath the satellite landing trajectory may include quite flat areas as in Figure 9, where rocks are rarely distributed and the approximate dimensions of the rocks, on which the satellite can perform first impact, are of the order of few centimeters. Differently, the lander may happen to encounter the surface first on a big rock, with average chord in the order of meters, so larger than the CubeSat itself, as in Figure 10. Initial coordinates are the DART crater nominal position and 4 sites surrounding it, still on the rocky area but close to its boundaries to consider for possible change in terrain profile along the trajectory, from rocky to flat when motion continues outside the rocky area. Changing the terrain encountered by the satellite during its motion is a realistic assumption based on the data about Itokawa

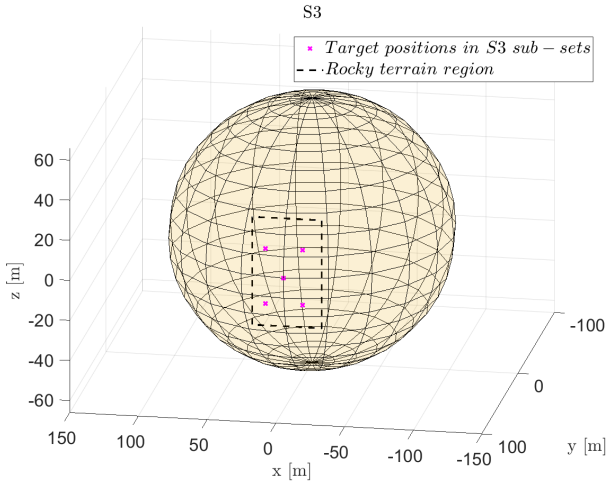


Fig. 8. S3 sub-sets fixed initial coordinates on the ellipsoid. Rocky area inside the dotted line.

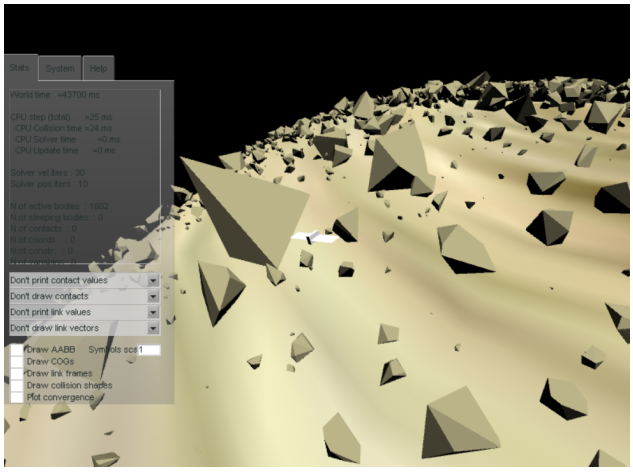

Fig. 9. Local terrain configuration in the nominal position (-10°, 80°) in Chrono simulation environment. The satellite falling will collide at first impact on few small rocks rarely distributed in the area. (Note: the Figure is taken from Project Chrono simulation rendering tool, the grey box on the left side can be ignored for the purposes of the Figure).

surface (Yano et al. (2006)). The latter is covered by two main types of soil: a very rocky one and quite a smooth one, this dichotomy is included for Dimorphos as flat and rough terrain profiles, since little information is available about Didymos terrain features. The study considers one possible terrain profile that combines superficial rugosity and flatness. The COR of the terrain is randomly varied to lower values in S3. The variation interval is between the worst-cases in literature, extremely elastic surface with COR of 0.85 close to Itokawa's one (Yano et al. (2006)) and extremely low COR of 0.1 as the one estimated for Eros surface in Tardivel et al. (2014).

So far the differences between each set of simulations have been described, but all the samples have some common inputs for initial height, velocity, orientation, spin and friction coefficient, given in Table 3. The trajectories simulated in the paper are the ending part of a passive landing. The complete landing trajec-

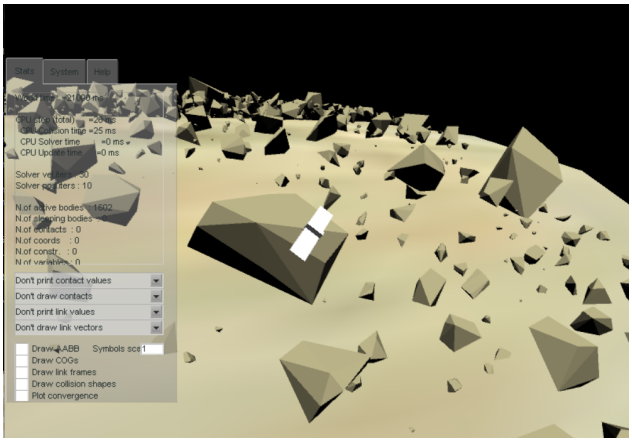


Fig. 10. Local terrain configuration in the nominal position (10°,100°) in Chrono simulation environment. The satellite falling will collide at first impact on the big rock right underneath it, which is even larger than the CubeSat itself. (Note: the Figure is taken from Project Chrono simulation rendering tool, the grey box on the left side can be ignored for the purposes of the Figure).

tory design of Milani, that starts from its operational orbit, has already been studied in previous documents (Ferrari & Lavagna (2018), Laino (2021)). So, the initial height range in Table 3 is the height from which the simulated fall is considered, close to the small body. Impact velocity module for Milani is expected in the order of few cm/s (Ferrari & Lavagna (2018)). So, the initial value is randomly varied between 1 cm/s and 8 cm/s, with upper bound chosen close to the estimated Dimorphos escape velocity in Ferrari & Lavagna (2018), and the velocity range is expected to be compatible with a successful landing, so managing to stay on surface. The initial velocity vector is directed towards the surface, putting the satellite on a trajectory intersecting the target. Random initial attitude and small spin rate are given to the probe adding realism to the descent approach (Van wal et al. (2018)). The coefficients of restitution and friction are constant in each sample. Milani's COR is the real value 0.6 given in Ferrari & Lavagna (2018). Friction coefficients are fixed in every set to 0.6, average value from literature (Van wal et al. (2018)). In fact, previous studies showed that the COF has less influence on the dynamics than the COR (Van wal et al. (2018), Van Wal (2014), Tardivel et al. (2014), Van Wal et al. (2017)). The simulation time and number of samples per set have been chosen as a compromise between computational time and cost. More than two hours is expected in Laino (2021) for landing on a flat surface in S1 , when starting the simulation from a farther distance, while S1 results show that 5000s (roughly 1 hour and 23 minutes) are more than enough, considering margins, for settling in most scenarios.

## 5. Results

Average results of performance are obtained for every set and shown in Table 4. The effect of rocks and trends in the results are investigated comparing the outcomes of each set.

### *5.1. Flat vs rocky terrain*

From the results of S1 and S2 sets, the effect of rocks on lander motion can be appreciated and considerations inferred to help the disposal design of the landing region and time.
Keeping in mind the goal to stay on surface after contact, the initial conditions have been set accordingly. A simulation is considered successful if the lander comes to rest on Dimorphos, with final velocity module below 1mm/s. Since the expected escape velocity is in the order of few cm/s, the rest condition is strictly set one order lower. The results obtained show that the imposed initial conditions to the campaign, in particular the initial velocity of the lander constrained below the expected escape threshold on surface, proved to be compatible with a successful landing and all the simulations managed to stay on Dimorphos' surface. From the performance results and statistical characterization of the campaign carried out, relevant outcomes for landing on an unknown terrain and for surface motion evolution can be inferred. Results show and quantify rough terrain effects: perturbation of the trajectory and increase of number of impacts, when lander's energy is dissipated.
Settling time is computed from the initial instant of descent up to the instant the velocity drops below 1mm/s on the surface. Comparing the values in Table 4 of S1 and S2 sets, time decreases when rocks are included. The rougher the soil is, the more the satellite motion is perturbed and energy is dissipated at each impact. The major effect of terrain irregularities on settling time can be noticed also comparing the S1 and S2 results with the mean settling time of set S3, decreasing the surface COR has a minor effect on the parameter with respect to targeting a rocky region than a flat one, even in extreme case conditions of elastic soil. Analysing the samples obtained, the settling time in the S1 set can reach up to 50 minutes, while in both the S2 and S3 sets, where rocks are included, the maximum settling time reachable, within the simulated environment, is limited to 40-45 minutes.
The bounding circle defined in Table 4 is the minimum-radius circle on the surface that circumscribes all the final rest sites in a set of simulations. Its radius is computed as the ellipsoid dihedral angle from the centre of this circle up to the farthest rest point obtained. The radius of the bounding circle is given in terms of latitude and longitude coordinates, while the maximum straight linear distance covered by the probe is computed from first impact site to rest position. The effect of rocks causes reduction of the dispersion area with respect to a flat surface. This influence on the dispersion area is relevant and comparable with the effect of a lower terrain COR investigated in S3 set. In fact the results of S3 set, in terms of bounding circle radius and maximum linear distance travelled by the lander, are affected by the presence of one single simulation in which Milani travels far on the surface (see the maximum data of the first column for S3 set in Table 4). The results in the second column of Table 4 for S3 set, cleared of this extreme sample, are closer to the ones caused by the elastic rocky terrain effect of S2. Reducing the distance travelled by the satellite during contact motion is beneficial when targeting a specific site on surface, such as the DART crater. Moreover, it limits the possibility that the lander moves to regions with lower escape velocity threshold.

Table 3. Input parameters to each set of simulations. Since some inputs are equal in all the sets they are reported only once in the Table and the column of the data is shared by all the sets. Differently, the peculiar inputs of each set of simulations are given in separate columns for each set.

| **Parameter** | **S1** | **S2** | **S3** |
|---|---|---|---|
| Initial longitude | [70°; 110°] | [75°; 105°] | (0°, 90°)<br>(10°, 80°)<br>(-10°, 80)<br>(-10°, 100°)<br>(10°, 100°) |
| Initial latitude | [-20°; 20°] | [-15°; 15°] | |
| Initial height | [2m; 10m] | | |
| Initial linear velocity | [1cm/s; 8cm/s] | | |
| Initial angular velocity | $1 \times 10^{-3}$rad/s | | |
| Milani COR | 0.6 | | |
| Terrain COR | 0.85 | | [0.1; 0.85] |
| Milani and terrain COF | 0.6 | | |
| Simulation time | 9000s | 5000s | |
| Number of simulations | 300 | 100 | 500 |

During the initial ballistic descent the satellite tends to equatorial latitude, while on surface motion there is no clear trend. The trends in motion evolution are highlighted in terms of coordinates variation on surface in Figure 11. In the S3 set of simulations it might be inferred some trend towards increasing longitudes of the lander's motion, that may be related to the local terrain configuration targeted, as will be better detailed in Section 5.2. A linear relation can be approximated between the surface distance covered and the number of hops of the probe and it is shown in Figure 12. A hop is defined when the satellite travels at least 1cm between two consecutive impacts on the surface, less than Milani's size $365.9 \times 226.3 \times 100$mm, later in the paper the distinction between bounces and rollings will be introduced, with the term hops we consider both bounces and rollings, without distinction. Linear fitting slopes confirm that the presence of rocks increases the number of motion perturbations with respect to a flat surface, when covering the same distance.

Before coming to a rest, the probe typically performs a rolling motion of successive small rebounces with no relevant distance travelled. In Figure 12 any hop covering more than 1cm on surface was detected, now a distinction is made between bounces and rollings. If a ballistic arc covers more than 1m, one

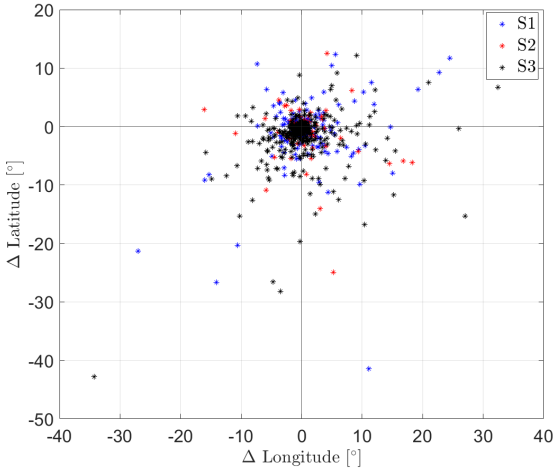


Fig. 11. Δ longitude and Δ latitude coordinates from first impact to rest position of each sample in S1, S2 and S3 sets. (Positive values of Δ latitude mean that the overall motion of the lander brought it closer to the equator, so final latitude closer to zero).

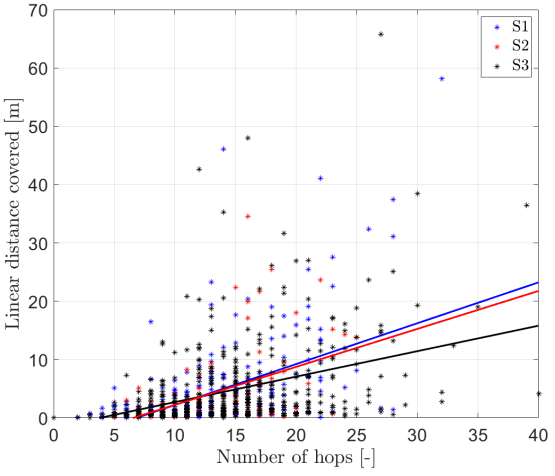


Fig. 12. Number of hops (any hop covering more than 1cm on the surface, later in the paper the distinction between bounces and rollings will be introduced) relations with the linear distance covered by simulations in S1, S2 and S3 sets. Linear fitting slopes of hops number and distance relations are (S1; S2; S3) = (0.70; 0.65; 0.44); lower slope means less distance traveled for same number of hops.

Table 4. Main results obtained in the analysis, for each set of simulations. The S3 column reports the average results of all the samples in the set (left column), and the results of the S3 samples without that one single simulation that managed to perform more than 65 m on surface (right column).

| | **S1** | **S2** | **S3** | **Reduced S3 results** |
|---|---|---|---|---|
| **Mean settling time** | 14min 33s | 13min 57s | 13min 54s | 13min 51s |
| **Bounding circle radius** | 47.2° | 29.1° | 43.9° | 36.2° |
| **Maximum linear distance** | 58.2m | 34.5m | 65.8m | 48m |
| **Mean angular distance** | 2.9° | 3.2° | 3.3° | 3.2° |
| **Mean linear distance** | 4.1m | 4.5m | 4.7m | 4.6m |
| **Mean number of bounces** | <1 (0.76) | <1 (0.82) | <1 (0.93) | <1 (0.92) |
| **Mean number of rollings** | 12 | 13 | 14 | 14 |
| **Mean distance of one bounce** | 3.3m | 4.1m | 3.5m | 3.5 m |
| **Mean velocity of one bounce** | 1.5cm/s | 1.7cm/s | 1.6cm/s | 1.6cm/s |
| **Mean velocity of one rolling** | 0.93cm/s | 0.98cm/s | 0.97cm/s | 0.97cm/s |
| **Percentage of samples with no bounces** | 56% | 51% | 47% | 47% |
| **Percentage of rollings after last bounce** | 87% | 86.8% | 85.6% | 85.7% |

order larger than the CubeSat dimensions, the lander is said to bounce, otherwise a step between 1cm and 1m is considered rolling. When Milani lands on an irregular soil in the simulated environment it is more probable that it performs a bouncing motion. As can be seen from the histograms in Figure 13, many simulations performed only one energetic jump on the smooth surface of S1 before rolling and coming to rest, differently, the distributions in Figure 13 for sets S2 and S3 show a significant number of simulations that performed even 2-4 bounces on the surface. Rollings data include the final path travelled by the lander, where it rolls up to rest, and the in-place reorientation of the satellite between bounces. Rocks favour rolling between bounces since the lander orientation changes with every impact. The smooth soil favours the final rolling path of the satellite on surface, while rocks perturb the satellite's motion and allow it

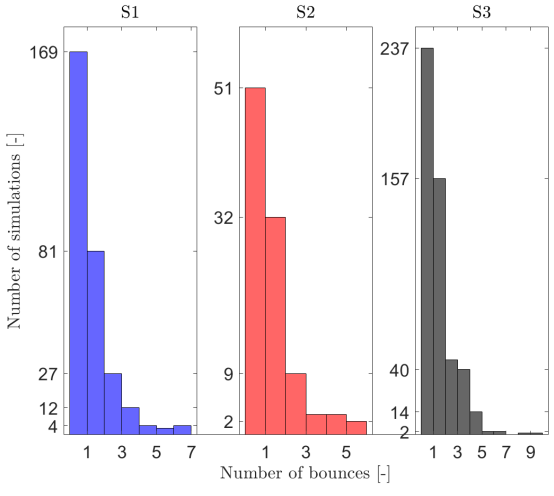


Fig. 13. Histogram that shows the distribution of number of bounces per sample in each set of simulations.

to get stuck on the terrain. In fact, the mean impact velocity of the rollings in the S1 simulations is lower than the S2 and S3 ones, and the average percentage of rollings after the last bounce in one simulation is higher when the lander moves on the smooth ellipsoid than when it travels through rocks.
In approximately half of the simulations in each set the satellite did not bounce on surface. Given the velocity of first impact considered, which is compatible with landing, the CubeSat in many cases undergoes only rolling motion on surface before coming to rest. As can be noticed from data in Table 4 the presence of rocks on the terrain favours bouncing and also the local terrain configuration has an important effect, as will be detailed in Section 5.2. In fact, as the complex 6-DOF dynamics of the lander is being considered, the orientation of impact influences much the evolution of the motion, due to coupling of normal-tangential effect. An irregular soil combined with the realistic shape of the CubeSat simulated result in higher aspect angle variability at impact.

### *5.2. Mixed topography*

S3 results in Table 5 focus on the effect of local terrain configuration and change of topography during the motion. Rocks effects are combined with a lower COR of the terrain, increasing the amount of probe's energy absorbed by the terrain per collision, according to the contact model implemented.

However, the effect of a rocky terrain (i.e. S2 compared to S1) is more significant than the effect of a less elastic soil.
More energy is dissipated per each contact in the S3 scenario, so settling time and dispersion area performance decrease with respect to the other cases in Table 4. The effect of soil configuration and terrain topography during motion emerge from Table 5. The effect of local terrain configuration on the evolution of surface motion can be inferred focusing on the samples of S3 with initial position set at (10°,100°). In fact, as shown in Figure 10, the lander targets the site on surface covered by a

Table 5. Main results obtained in the analysis for the successful simulations in each sub-set of S3. The (10°,100°) column reports the average results of all the samples in the sub-set (left column), and the results of the sub-set without that one single simulation that managed to perform more than 65 m on surface (right column).

| | **(0°, 90°)** | **(10°, 80°)** | **(-10°, 80°)** | **(-10°, 100°)** | **(10°, 100°)** | |
|---|---|---|---|---|---|---|
| **Mean settling time** | 13min 24s | 13min 36s | 13min 55s | 13min 4s | 15min 29s | 15min 12s |
| **Bounding radius** | 19.0° | 17.7° | 17.5° | 20.6° | 35.2° | 21.3° |
| **Maximum linear distance** | 42.6m | 36.4m | 35.3m | 48.0m | 65.8m | 39.5m |
| **Mean angular distance** | 2.3° | 3.1° | 3.2° | 2.3° | 5.4° | 5.0° |
| **Mean linear distance** | 3.3m | 4.4m | 4.5m | 3.3m | 8.0m | 7.4m |
| **Mean number of bounces** | <1 (0.62) | <1 (0.76) | <1 (0.88) | <1 (0.60) | >1 (1.79) | >1 (1.27) |
| **Mean number of rollings** | 12 | 15 | 14 | 12 | 15 | 15 |
| **Percentage of samples with no bounces** | 62% | 56% | 47% | 60% | 12% | 12% |

large rock right underneath it and this causes an energetic impact on the boulder and bouncing of the satellite. The bounce may allow it to cover large distance on surface, as proved by the average data in Table 5, in terms of distance covered, bouncing motion characteristics and less percentage of samples that stop without bouncing.

Observing the latitude and longitude variations on surface with respect to the S3 set in Figure 14, general trends in the motion of the lander can be investigated, as motion towards higher latitudes, that prevails when starting from positive latitudes, and motion towards increasing longitudes, that prevails when starting from negative latitudes. In fact, simulations that targeted the site at (-10°, 80°) on surface, mainly developed on rough terrain. This sub-set shows a smaller dispersion area and more energetic bounces than the sub-sets targeting the other sites, in which many samples moved from the rocky region to the smooth ellipsoid in the surroundings. From the data in Table 5 it is inferred that the local terrain configuration plays a significant role on the motion evolution, as proved by the data for samples starting at (10°,100°) that differ from the other sub-sets of set S3.

The resulting mean time needed for CubeSat Milani to come to rest on Dimorphos can be set around 15 minutes covering an average distance of 4-5m, considering the COR interval of S3. In average Milani is expected to bounce once on surface, which is more probable if the landing site is rocky, and roll up to rest. The investigated impact velocity is compatible with a successful landing, as expected from previous results on the estimated escape velocity threshold.

As mentioned, the terrain COR is not fixed for all simulations in the S3 set. This numerical coefficient is provided to set up the terrain material property in Chrono and is different from the global COR that includes both terrain and lander effects. The latter is computed at post-processing level, by using equations 10 and 11 applied to the results of each simulation, and shown per each sample in Figure 15. We define a kinetic COR, as the ratio between the probe velocity after and before collision (eq. 10), and an energetic COR, as the ratio between the lander's energy after and before the collision, both translational and rotational contributions (eq. 11).

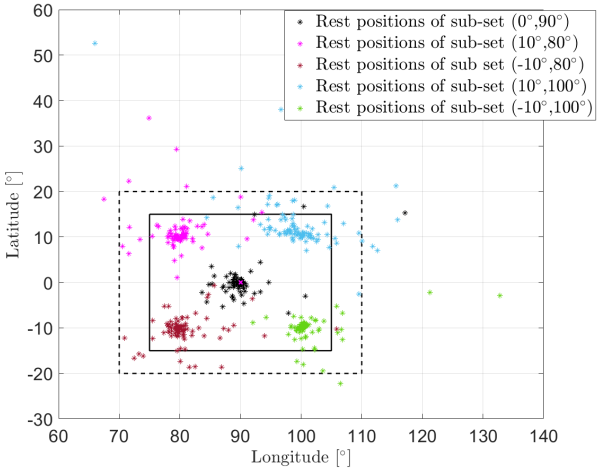


Fig. 14. The Figure shows the final resting sites on surface of each sample in every seb-set of simulations of S3, identified by different colors. The black continuous line is the region of possible initial position of set S2, that includes the targeted locations on surface in S3. The black dotted line defines the rocky region simulated.

$$COR_{kinetic} = \\ = \frac{velocity\ after\ impact}{velocity\ before\ impact} \tag{10}$$

$$COR_{energetic} = \\ = \frac{(E_{translation} + E_{rotation})_{after\ impact}}{(E_{translation} + E_{rotation})_{before\ impact}} \tag{11}$$

The kinetic definition takes into account only the point translational velocity variation at contact. This is a typical approach in literature when dealing with point-masses, but when dealing with full 6-DOF dynamics the energetic definition is more accurate. The overall energetic COR includes the rotational energy that is not bound to decrease at each collision and it hardly goes below 0.6, which is exactly the lander's COR in Chrono. When

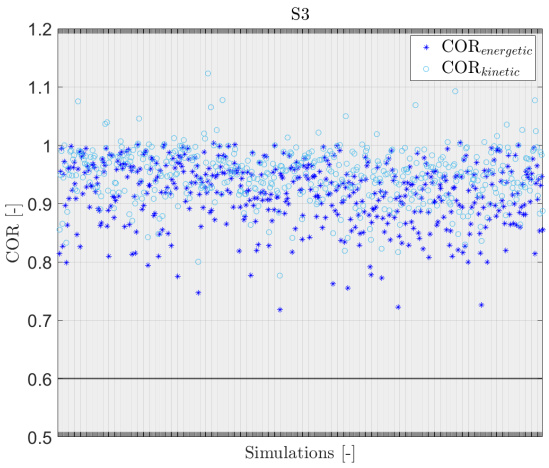


Fig. 15. Kinetic (o) and energetic (∗) COR computed for each simulation of S3 set. The horizontal line is the 0.6 COR value of Milani's structure.

the asteroid's COR is high it is the main contribution to the energetic parameter, while the satellite's coefficient has the major effect when the soil's one is low. The lander's COR partially mitigates terrain variability.
In addition to the rocky terrain effect, the restitution coefficient is found to influence the satellite landing. The information on these characteristics of the soil should be combined to design a successful and robust disposal for Milani on Dimorphos.

## 6. Discussion

The performance parameters inferred from the three sets of simulations show the importance of the presence of rocks compared to a flatter soil. Tardivel et al. (2014) and Van Wal et al. (2019) had already concluded how rocks increase trajectory variability, when modelled in the dynamical environment, respectively as physical obstacles through persistent rocks generation technique or as stochastic impulses during motion. A perturbed motion on an irregular soil can give valuable measurements from the on-board instrumentation about surface characteristics, as happened for Hayabusa and Rosetta missions (Yano et al. (2006), Biele et al. (2015)). Adding rocks to the environment reduces the mean settling time, and even more when the soil COR is below the extreme case of 0.85. However, it must be pointed out how the local terrain configuration plays a fundamental role on the landing performance. These data help with landing site and time choice; reducing the time needed to land could be beneficial to perform a surface experiment before passivation. Considerations are made on the dispersion area: a rocky soil favours the bouncing motion of the lander and allows for energetic impacts that may cover significant distances on surface and still manage to come to rest on Dimorphos, given the range of impact velocity. The results are in accordance with the outcomes in Van Wal et al. (2019) and Van Wal et al. (2017) stating how impacts on rocks randomize the local normal direction at each bounce. This is enforced by our use of a realistic shape for the lander whose attitude at different impacts varies the velocity direction at contact point, as discussed in Van Wal et al. (2019) in terms of higher aspect angle variability compared to spherical shapes.
Two other major effects on the contact dynamics of the lander are the local terrain conformation and the COR of the soil. Settling time and dispersion area performance depend on the local topography of the landing site, as proved by the single nominal trajectories analyzed in S3. When considering the effect of mixed topography simulated, the trends in motion evolution seen in the data cause many samples to move from the rocky region to the smooth surface in the surroundings, this influences the dispersion area of landing and the bouncing motion. The COR of the terrain represents the physical characteristics of the soil and, in addition to the topography, is another main parameter influencing the design of the landing.

## 7. Conclusions

The paper describes the modelling and simulation procedure of a CubeSat landing on an asteroid, with focus on the contact motion. The aim was to investigate the effects of a rocky soil and estimate landing performance, as well as the most relevant effects on the dynamics of the probe.
The simulation procedure described has general validity, and applies to the problem of small-body landing. The method aims at combining a realistic simulation environment, constrained by the available data of the case studied, with an acceptable computational cost.
As a study case, we investigated the problem of Milani CubeSat which is planned to land on Dimorphos at its end-of-life, targeting the DART crater region on the surface. The simulation exploits the built-in Chrono algorithms for dynamics integration and to solve contact dynamics. Milani is modelled as a 6-DOF rigid body, using its realistic shape. Dimorphos asteroid is modelled as a tri-axial ellipsoid with convex hulls randomly put on a limited surface area to reproduce rocks. The dynamical environment includes Didymos primary central gravity perturbed by spherical harmonics, Dimorphos shape-based gravity, apparent rotation forces and contact interactions between rigid and elastic surfaces: the normal non-penetration reaction and the tangential Coulomb friction, both parameterized by scalar coefficients. Since there is little knowledge on Dimorphos physical characteristics, three sets of simulations considered different scenarios. The satellite moved towards a flat terrain and a rocky one. A worst-case scenario is investigated with rigid and elastic soil and also a more realistic one in terms of higher energy absorbed by the terrain per impact.
Changes in performance parameters in the rocky scenario, with respect to the flat one, have been inferred. The settling time and the dispersion area are more limited when Milani is simulated to land on an irregular soil. The presence of rocks perturbs contact motion, increasing the number of impacts; in fact motion perturbations increase with respect to a flat surface, when considering the same distance covered. Some trends in the motion evolution in terms of direction of travel have been found, but significantly influenced by the local terrain configuration considered. Landing showed to be feasible even with no bouncing

motion on surface and the expected acceptable velocity range for successfully landing has been confirmed with the obtained results. An irregular soil would allow Milani to bounce on surface and to undergo many impacts with the terrain, which would be beneficial for instruments' measurements, and still come to rest permanently on surface. The described effects of a rocky terrain on the performance have been quantified for the case at hand. The obtained results for Milani landing on Dimorphos will help in the design of the best landing site, time and trajectory options, depending on the targeted mission goals. Moreover, two important effects have been proved to have a relevant influence on the lander contact dynamics: the local terrain configuration with change in the topography during motion and the effect of the terrain COR. Many assumptions have been made during the study. The analysis can be further extended in the future, both to a higher degree of accuracy and to investigate the influence of different parameters and scenarios. The images captured during the DART impact (Handal et al. (2022)) showed an irregular soil of Dimorphos. The surface characterisation from the recently obtained data is currently ongoing and will prove crucial to select the ideal landing site for Milani, in view of the expected effects of the terrain and of the future estimates on surface characteristics.

## References


Antreasian, P., Chesley, S., Miller, J. et al. (2001). The design and navigation of the near shoemaker landing on eros. *Advances in the Astronautical Sciences*, .

Biele, J., Ulamec, S., Maibaum, M. et al. (2015). Cometary science. the landing(s) of philae and inferences about comet surface mechanical properties. *Science (New York, N.Y.)*, *349*. doi:10.1126/science.aaa9816.

Cheng, A., Atchison, J., Kantsiper, B. et al. (2015). Asteroid impact and deflection assessment mission. *Acta Astronautica*, *115*, 262–269. URL: https://www.sciencedirect.com/science/article/pii/S0094576515002040. doi:https://doi.org/10.1016/j.actaastro.2015.05.021.

Cheng, A. F., Rivkin, A. S., Michel, P. et al. (2018). Aida dart asteroid deflection test: Planetary defense and science objectives. *Planetary and Space Science*, *157*, 104–115. URL: https://www.sciencedirect.com/science/article/pii/S0032063317304579. doi:https://doi.org/10.1016/j.pss.2018.02.015.

Ferrari, F., Franzese, V., Pugliatti, M. et al. (2021a). Preliminary mission profile of hera's milani cubesat. *Advances in Space Research*, *67*(6), 2010–2029. URL: https://www.sciencedirect.com/science/article/pii/S0273117720309078. doi:https://doi.org/10.1016/j.asr.2020.12.034.

Ferrari, F., Franzese, V., Pugliatti, M. et al. (2021b). Trajectory options for hera's milani cubesat around (65803) didymos, . *68*(4), 973–994. URL: https://doi.org/10.1007/s40295-021-00282-z. doi:10.1007/s40295-021-00282-z.

Ferrari, F., & Lavagna, M. (2018). Ballistic landing design on binary asteroids: The aim case study. *Advances in Space Research*, *62*(8), 2245–2260. URL: https://www.sciencedirect.com/science/article/pii/S027311771730844X. doi:https://doi.org/10.1016/j.asr.2017.11.033. Past, Present and Future of Small Body Science and Exploration.

Ferrari, F., Lavagna, M., & Blazquez, E. (2019). A parallel-GPU code for asteroid aggregation problems with angular particles. *Monthly Notices of the Royal Astronomical Society*, *492*(1), 749–761. URL: https://doi.org/10.1093/mnras/stz3458. doi:10.1093/mnras/stz3458.

Handal, J., Surowiec, J., & Buckley, M. (2022). Nasa's dart mission hits asteroid in first-ever planetary defense test. *Latest NASA News Releases*, . URL: https://www.nasa.gov/press-release/nasa-s-dart-mission-hits-asteroid-in-first-ever-planetary-defense-test.

Jurado, E., Martin, T., Canalias, E. et al. (2016). Rosetta lander philae: Flight dynamics analyses for landing site selection and post-landing operations. *Acta Astronautica*, *125*. doi:10.1016/j.actaastro.2016.03.030.

Laino, M. A. (2021). *Design of Landing Trajectories on Small Bodies with Application to Milani CubeSat in Didymos Binary Asteroid*. Master's thesis Politecnico di Milano. URL: http://hdl.handle.net/10589/176153.

Lauretta D.S., B. C. e. a., DellaGiustina D.N. (2019). The unexpected surface of asteroid (101955) bennu. *Nature*, *568*. doi:10.1038/s41586-019-1033-6.

Mazhar, H., Heyn, T., Pazouki, A. et al. (2013). Chrono: a parallel multi-physics library for rigid-body, flexible-body, and fluid dynamics. *Mechanical Sciences*, *4*(1), 49–64. URL: https://ms.copernicus.org/articles/4/49/2013/. doi:10.5194/ms-4-49-2013.

Michel, P., Cheng, A., Küppers, M. et al. (2016). Science case for the asteroid impact mission (aim): A component of the asteroid impact & deflection assessment (aida) mission. *Advances in Space Research*, *57*(12), 2529–2547. URL: https://www.sciencedirect.com/science/article/pii/S0273117716300692. doi:https://doi.org/10.1016/j.asr.2016.03.031.

Michel, P., Kueppers, M., Sierks, H. et al. (2018). European component of the aida mission to a binary asteroid: Characterization and interpretation of the impact of the dart mission. *Advances in Space Research*, *62*(8), 2261–2272. URL: https://www.sciencedirect.com/science/article/pii/S0273117717308967. doi:https://doi.org/10.1016/j.asr.2017.12.020. Past, Present and Future of Small Body Science and Exploration.

Naidu, S., Benner, L., Brozovic, M. et al. (2020). Radar observations and a physical model of binary near-earth asteroid 65803 didymos, target of the dart mission. *Icarus*, *348*, 113777. URL: https://www.sciencedirect.com/science/article/pii/S0019103520301640. doi:https://doi.org/10.1016/j.icarus.2020.113777.

Rivkin, A. S., Chabot, N. L., Stickle, A. M. et al. (2021). The double asteroid redirection test (DART): Planetary defense investigations and requirements. *The Planetary Science Journal*, *2*(5), 173. URL: https://doi.org/10.3847/psj/ac063e. doi:10.3847/psj/ac063e.

Scheeres, D. (1994). Dynamics about uniformly rotating triaxial ellipsoids: Applications to asteroids. *Icarus*, *110*(2), 225–238. URL: https://www.sciencedirect.com/science/article/pii/S0019103584711183. doi:https://doi.org/10.1006/icar.1994.1118.

Scheeres, D., Van wal, S., Olikara, Z. et al. (2019). Dynamics in the phobos environment. *Advances in Space Research*, *63*(1), 476–495. URL: https://www.sciencedirect.com/science/article/pii/S0273117718307853. doi:https://doi.org/10.1016/j.asr.2018.10.016.

Tardivel, S., Scheeres, D. J., Michel, P. et al. (2014). Contact motion on surface of asteroid. *Journal of Spacecraft and Rockets*, *51*(6), 1857–1871. URL: https://doi.org/10.2514/1.A32939. doi:10.2514/1.A32939.

Tasora, A., & Anitescu, M. (2010). A Convex Complementarity Approach for Simulating Large Granular Flows. *Journal of Computational and Nonlinear Dynamics*, *5*(3). URL: https://doi.org/10.1115/1.4001371. doi:10.1115/1.4001371. 031004.

Tasora, A., Serban, R., Mazhar, H. et al. (2016). Chrono: An open source multi-physics dynamics engine. In T. Kozubek, R. Blaheta, J. Šístek, M. Rozložník, & M. Čermák (Eds.), *High Performance Computing in Science and Engineering* (pp. 19–49). Cham: Springer International Publishing.

Tsuda, Y., Saiki, T., Terui, F. et al. (2020). Hayabusa2 mission status: Landing, roving and cratering on asteroid ryugu. *Acta Astronautica*, *171*. doi:10.1016/j.actaastro.2020.02.035.

Van Wal, S. (2014). *The Ballistic Deployment of Asteroid Landers*. Master's thesis TU Delft. URL: http://resolver.tudelft.nl/uuid:20f07d7e-3d2d-498a-898a-e165affa6c12.

Van Wal, S., Reid, R., & Scheeres, D. (2019). Simulation of nonspherical asteroid landers: Contact modeling and shape effects on bouncing. *Journal of Spacecraft and Rockets*, *57*, 1–22. doi:10.2514/1.A34573.

Van Wal, S., & Tardivel (2016). High-fidelity small-body lander simulations. *6th International Conference on Astrodynamics Tools and Techniques*, .

Van Wal, S., Tardivel, S., & Scheeres, D. (2017). Parametric study of ballistic lander deployment to small bodies. *Journal of Spacecraft and Rockets*, *54*(6), 1330–1355. URL: https://doi.org/10.2514/1.A33832. doi:10.2514/1.A33832.

Van wal, S., Tsuda, Y., Yoshikawa, K. et al. (2018). Prearrival deployment

analysis of rovers on hayabusa2 asteroid explorer. *Journal of Spacecraft and Rockets*, *55*(4), 797–817. URL: https://doi.org/10.2514/1.A34157. doi:10.2514/1.A34157.

Wen, T., & Zeng, X. (2022). Natural landing dynamics near the secondary in single-tidal-locked binary asteroids. *Advances in Space Research*, *69*(5), 2223–2239. URL: https://www.sciencedirect.com/science/article/pii/S0273117721009315. doi:https://doi.org/10.1016/j.asr.2021.12.021.

Wen, T., Zeng, X., Circi, C. et al. (2020). Hop reachable domain on irregularly shaped asteroids. *Journal of Guidance, Control, and Dynamics*, *43*(7), 1269–1283. URL: https://doi.org/10.2514/1.G004682. doi:10.2514/1.G004682.

Yano, H., Kubota, T., Miyamoto, H. et al. (2006). Touchdown of the hayabusa spacecraft at the muses sea on itokawa. *Science*, *312*(5778), 1350–1353. URL: https://science.sciencemag.org/content/312/5778/1350. doi:10.1126/science.1126164.

Zannoni, M., Tommei, G., Modenini, D. et al. (2018). Radio science investigations with the asteroid impact mission. *Advances in Space Research*, *62*(8), 2273–2289. URL: https://www.sciencedirect.com/science/article/pii/S0273117717308773. doi:https://doi.org/10.1016/j.asr.2017.12.003. Past, Present and Future of Small Body Science and Exploration.

Zeng, X., Wen, T., Li, Z. et al. (2022a). Natural landing simulations on generated local rocky terrains for asteroid cubic lander. *IEEE Transactions on Aerospace and Electronic Systems*, (pp. 1–1). doi:10.1109/TAES.2022.3152099.

Zeng, X. Y., Li, Z. W., Wen, T. G. et al. (2022b). Influence of the lander size and shape on the ballistic landing motion. *Earth and Space Science*, *9*(2), e2021EA001952. URL: https://agupubs.onlinelibrary.wiley.com/doi/abs/10.1029/2021EA001952. doi:https://doi.org/10.1029/2021EA001952. arXiv:https://agupubs.onlinelibrary.wiley.com/doi/pdf/10.1029/2021EA001952. E2021EA001952 2021EA001952.

Zhang, L., Jin, X., & He, H. (1999). Prediction of fragment number and size distribution in dynamic fracture. *Journal of Physics D: Applied Physics*, *32*(5), 612–615. URL: https://doi.org/10.1088/0022-3727/32/5/017. doi:10.1088/0022-3727/32/5/017.

Zhang, Y., Li, J., Zeng, X. et al. (2021). High-fidelity landing simulation of small body landers: Modeling and mass distribution effects on bouncing motion. *Aerospace Science and Technology*, *119*, 107149. URL: https://www.sciencedirect.com/science/article/pii/S1270963821006593. doi:https://doi.org/10.1016/j.ast.2021.107149.